Available online at www.sciencedirect.com

SCIENCE DIRECT

Developmental Biology 284 (2005) 421 – 436

DEVELOPMENTAL BIOLOGY

www.elsevier.com/locate/ydbio

A mutation in the *silver* gene leads to defects in melanosome biogenesis and alterations in the visual system in the zebrafish mutant *fading vision*

Helia B. Schonthaler[a], Johanna M. Lampert[b], Johannes von Lintig[b], Heinz Schwarz[c], Robert Geisler[c], Stephan C.F. Neuhauss[a,*]

[a]*Swiss Federal Institute of Technology, Department of Biology, and Brain Research Institute of the University of Zurich, Winterthurerstrasse 190, CH-8057 Zurich, Switzerland*

[b]*Neurobiology, Institute of Biology I, University of Freiburg, D-79104 Freiburg, Germany*

[c]*Max-Planck-Institut für Entwicklungsbiologie, Spemannstrasse 35, D-72076, Tübingen, Germany*

Received for publication 17 August 2004, revised 1 June 2005, accepted 1 June 2005
Available online 15 July 2005

Abstract

Forward genetic screens have been instrumental in defining molecular components of visual function. The zebrafish mutant *fading vision* (*fdv*) has been identified in such a screen due to defects in vision accompanied by hypopigmentation in the retinal pigment epithelium (RPE) and body melanocytes. The RPE forms the outer most layer of the retina, and its function is essential for vision. In *fdv* mutant larvae, the outer segments of photoreceptors are strongly reduced in length or absent due to defects in RPE cells. Ultrastructural analysis of RPE cells reveals dramatic cellular changes such as an absence of microvilli and vesicular inclusions. The retinoid profile is altered as judged by biochemical analysis, arguing for a partial block in visual pigment regeneration. Surprisingly, homozygous *fdv* vision mutants survive to adulthood and show, despite a persistence of the hypopigmentation, a partial recovery of retinal morphology. By positional cloning and subsequent morpholino knock-down, we identified a mutation in the *silver* gene as the molecular defect underlying the *fdv* phenotype. The Silver protein is required for intralumenal fibril formation in melanosomes by amylogenic cleavage. Our data reveal an unexpected link between melanosome biogenesis and the visual system, undetectable in cell culture.

Keywords: *Danio rerio*; Melanosome; Retinal pigment epithelium; Visual cycle; Photoreceptor; *Silver*; Pmel17

Introduction

The perception of light by the vertebrate retina depends critically on cellular interactions between the retinal pigment epithelium (RPE) and the light gathering photoreceptors. Photons are absorbed by photopigments in the outer segments of photoreceptor cells (PRC), triggering a signaling cascade ultimately leading to a decrease in glutamate release at the photoreceptor ribbon synapse (Rodieck, 1998). The PRC outer segments are closely associated with the RPE, with microvilli of the RPE interdigitating between the PRCs, and both cell types cooperate on multiple aspects of vision.

The RPE forms the outer most layer of the retina, accomplishing many supporting functions essential for the function and survival of photoreceptors. These functions include the transport of nutrients, the synthesis of the interphotoreceptor matrix, retinoid processing and circadian phagocytosis of shed PRC outer segments. Given these diverse roles of the RPE in normal visual function, it comes as no surprise that a growing number of outer retinal diseases are attributed to defects in the RPE (Bok, 1985, 1993; Pacione et al., 2003).

In an attempt to identify essential genes for vertebrate visual function, we have screened a collection of zebrafish mutants for defects in visually evoked optokinetic eye movements (Neuhauss et al., 1999) and identified the

* Corresponding author. Fax: +41 1 635 3303.
E-mail address: neuhauss@hifo.unizh.ch (S.C.F. Neuhauss).

0012-1606/$ - see front matter © 2005 Elsevier Inc. All rights reserved.
doi:10.1016/j.ydbio.2005.06.001

mutant *fading vision (fdv)* that displays a reduced optokinetic activity following visual stimulation. This mutant was originally isolated during a large-scale chemical mutagenesis screen (Haffter et al., 1996) by virtue of its pale eye and body pigmentation (Kelsh et al., 1996). Our morphological analysis of *fdv* revealed defects in melanosome biogenesis resulting in hypopigmentation of melanocytes and RPE cells with intracellular vesicular inclusions. The PRC outer segments are significantly reduced, and the recycling of visual pigment is impaired in *fdv* mutant larvae, as judged by a biochemical analysis of visual cycle intermediates. Surprisingly, despite the persistence of the melanocyte phenotype, the RPE recovers during post-larval development. Homozygous adult *fdv* fish have morphologically normal retinas with hypopigmented RPE cells and PRC outer segments nearly reaching wild-type length.

Fine mapping of the mutation leads to the identification of a candidate gene encoding for the type I integral membrane protein *silver a* (*silva*). Subsequent sequencing of the mutated and wild-type alleles as well as morpholino knock-down experiments have identified this locus as the gene altered by the *fdv* mutation. Consistent with the *fdv* phenotype, *silva* is exclusively expressed in melanocytes and RPE cells. In these cells, it is crucial for the formation of the intralumenal fibrous striations in early melanosomes on which melanin is polymerized. Formation of the intralumenal fibrils requires the cleavage of the mammalian Silver protein by a proprotein convertase. Recently, it has been shown that such cleavage regulates melanosome biogenesis by controlling the fibrillogenic activity (Berson et al., 2003; Kelly and Balch, 2003). The process of naturally occurring and functional *Silv* fiber formation in melanosomes is comparable to pathological processes of amyloidogenesis, as for example seen for gelsolin associated with familial type amyloidosis of Finnish type (FAF) (Huff et al., 2003; Ratnaswamy et al., 1999) and in Alzheimer's disease (Berson et al., 2003).

We additionally identified a second paralogue of *silver*, *silver b* (*silvb*), expressed in RPE cells but not in melanocytes.

Our data identify *fdv* as the first molecularly characterized zebrafish model of a melanosome biogenesis mutant, providing an unexpected link to visual system development.

Materials and methods

Zebrafish maintenance and strains

Zebrafish were bred and maintained under standard conditions at 28°C (Brand and Nüsslein-Volhard, 2002). Morphological features characteristic of developmental stages were used to determine the stage of the embryos in hours post-fertilization (hpf), according to Kimmel et al. (1995).

Mapping and cloning of fading vision

The *fading vision* (*fdv*), th236a mutation was assigned to linkage group 11 by using a panel of 192 simple sequence length polymorphisms (SSLP) markers distributed over the whole genome. Pooled segregate analysis was performed as described earlier (Geisler, 2002) on pooled DNA isolated from 48 homozygous *fdv* mutant larvae and pooled DNA of 48 control siblings from the same cross. Since the *fdv* mutation was induced in the Tü strain, the WIK strain was used as the mapping strain. Further fine mapping was performed using the total DNA of 1223 homozygous mutant single embryos of different map crosses.

ESTs (Geisler et al., 1999; Hukriede et al., 2001) located in the same interval as the *fdv* mutation were identified and analyzed on precast SSCP (single strand conformation polymorphisms) gels (ETC Elektrophorese Technik, Kirchentellinsfurt, Germany). SSCP gels were run horizontally for 20 min at 15°C and for approximately 1.5 h at 7°C (setup by ETC Elektrophorese Technik, Kirchentellinsfurt, Germany). Additionally, all PCR products that showed a recombination event on the SSCP gel when tested with the closest SNP marker were sequenced to verify the SSCP result.

BAC library screens and radiation hybrid mapping

PCR pools of two zebrafish genomic BAC libraries, DanioKey and Chori211, were screened by PCR. The BAC end sequences were used to design primers for radiation hybrid mapping (RH mapping). The RH mapping served to exclude any false positive BACs isolated in the library screen.

BACs and ESTs were mapped on the Goodfellow T51 RH panel (Geisler et al., 1999). Appropriate primers were designed and PCRs were run on the RH panel. For all markers, the PCR was done independently in duplicates.

Cloning and sequencing of silva and silvb

To identify the molecular defect underlying the *fdv* phenotype, total RNA of 72 hpf wild-type and *fdv* mutant zebrafish embryos, as well as total RNA of adult wild-type and *fdv* mutant zebrafish eyes were isolated and reverse transcribed using oligo(dT) primers (SuperScript™ II, Invitrogen, Switzerland). The resulting cDNA was used for PCR in order to amplify the candidate gene. Primers for the amplification were designed based on the sequences of ESTs fj24g11, fj03d05 and fc11g11 (Clark et al., 2001) obtained by BLAST searches using the mouse and human Silv protein sequence. The wild-type coding sequence (cds) of the zebrafish *silva* was submitted to GenBank (AY554264).

To identify the mutation in *fdv*, amplification products were sequenced in fragments of 500 to 700 bp, obtained from both wild-type and *fdv* mutant larvae and from eyes of

adult fish. Sequencing was performed for PCR products derived from several independent PCR reactions. The sequences obtained were aligned and analyzed using the SeqMan program (DNAstar). The cds of the zebrafish *silvb* gene was also amplified from cDNA of 72 hpf old wild-type zebrafish embryos using primers designed on the predicted cds sequence (http://www.ensembl.org/Danio_rerio/) and subsequently cloned and sequenced. The cds sequence of *silvb* obtained was also submitted to GenBank (AY864065).

RNA probes and whole mount in situ hybridization

Embryos to be used for in situ hybridization were treated with 3 μM PTU (1-phenyl-2-thiourea (Sigma)) to prevent melanization. PTU-treated embryos were collected at different stages of development and staged by morphology (Kimmel et al., 1995). The embryos were fixed in paraformaldehyde (4% in PBS, pH 7.25) and incubated at 4°C overnight. Subsequently, the embryos were dehydrated in a methanol series and stored in methanol at −20°C. In situ hybridization was performed as described in Schulte-Merker (2002). Adult eyes were taken from albino fish. Fresh frozen 25 μm sections were air dried for half an hour and subsequently fixed in 4% paraformaldehyde (4% in PBS, pH 7.25). After washing in PBS, the sections were acetylated with triethanolamine and acetic anhydride in distilled water for 10 min. Subsequently, the sections were prehybridized for 3 h at 58°C. Hybridization was done overnight at 58°C in a humid chamber. After several washes with Saline–Sodium Citrate (SSC) at the hybridization temperature, the sections were blocked for 1 h.

Localization of *silva* and *silvb* mRNA by in situ hybridization was performed using digoxigenin-labeled antisense RNA probes and detection with Dig-specific antibodies. Plasmids for in situ probe synthesis were linearized, and riboprobes were generated with the DigRNA labeling kit (Roche Molecular Biochemicals) according to the manufacturer's instructions.

TUNEL assay

Cell death was detected by the TUNEL (TdT-mediated dUTP nick-end labeling) method on 25 μm cryosections, according to manufacturer's protocol (Cell Death Kit; Roche Molecular Biochemicals).

Histological analyses

For light microscopy (LM), larvae were fixed in 4% paraformaldehyde in PBS (pH 7.2) at 4°C overnight and washed in PBS. The embryos were dehydrated in an ethanol series, infiltrated and embedded in Technovit 7100 (Heraeus Kulzer, Germany) for sectioning. 3 μm sections of different developmental stages of mutant and wild-type larvae were cut with a glass knife and mounted on Superfrost Plus slides (Microm International, Switzerland). The sections were subsequently stained with 0.5% Toluidine blue in 1% in Borax buffer.

For ultrastructural analysis by transmission electron microscopy (TEM), larvae and eyes of adult zebrafish were fixed in 2% paraformaldehyde and 2.25% glutaraldehyde in PBS (pH 7.2) at 4°C overnight and subsequently washed in PBS. Larvae and eyes of adult fish were then dehydrated through a standard ethanol series and infiltrated with Epon. Sections through the head of the larvae or eyes of adult fish were collected on coated slot grids and examined in a Philips CM 10 electron microscope TEM.

Morphometry and statistical analyses

TEM sections were prepared as described above from 5-dpf-old mutant and wild-type larvae and from adult homozygous *fdv* mutant and age-matched wild-type zebrafish. Only transversal sections from the area surrounding the optic nerve in larval eyes and adult eyes were evaluated. A standard point-counting method was used to estimate the area of RPE, PRC outer segments. Additionally, the area of the PRC nuclei was calculated as an internal reference. The point-counting method allows determination of the area covered by a structure of interest. For that purpose, a grid of equally spaced points of defined size was superimposed to TEM sections taken from 5-dpf-old larval and age-matched adult zebrafish eyes. Points were approximately 1.2 μm and 2.1 μm spaced on larval and adult sections, respectively. The grid covers an area of approximately 528 μm^2 and 3500 μm^2 in the larval and adult retina, respectively. The grid was randomly superimposed on the area of interest (RPE, PRC outer segments, PRC nuclei), and the points covering the area of interest were counted. The data obtained were averaged and evaluated by a Student's *t* test.

Retinotectal projection

For dye injection, 5-day- and 6-day-old larvae were fixed in 4% paraformaldehyde in PBS (pH 7.2) at 4°C overnight then mounted in agarose (1.5% agarose in PBS) on a glass slide. DiI (1, 1′-dioctadecyl-3, 3, 3′, 3′-tetramethyl indocarbocyanine perchlorate; Molecular Probes, Invitrogen AG, Switzerland) was pressure injected in one eye of the larvae, and the resulting labeling evaluated after overnight incubation.

Morpholino injection

A morpholino antisense oligonucleotide was designed against the ATG region of the zebrafish *silva* mRNA. The sequence of the morpholino starts one base pair before the ATG start codon and has a length of 25 bp: GAGGAAGATGAGAGATGTCCACATG. The morpholino was injected in one-cell wild-type embryos at an oligonucleotide concentration of 100 μM and a pressure of 30 hP for 1 ms. As a control experiment, the control morpholino provided

by GenTools was injected into embryos at the one-cell stage using the same conditions.

Light microscopy

Light microscopic pictures were taken on an *Axioskop 2 Mot* microscope connected to an *AxioCam color* using the *AxioVision 3.0* software (Zeiss, Switzerland).

Analyses of the retinoid composition of the eyes by HPLC analyses

To determine the retinoid content of 7 dpf larval eyes and adult fish, eyes were illuminated for 10 min at 10,000 lx and then dark-adapted for 45 min. After the addition of ice to the fish water, the eyes were manually removed under binocular control and monochromatic light (695 nm). Eyes (50 larval heads or one pair of eyes from adult zebrafish) were transferred into a loose-fitting glass potter, and 200 μl of 2 M NH_2OH (pH 6.8) and 200 μl methanol were added, and the eyes were homogenized. From the resulting homogenate, retinoids were extracted under red safety light as previously described (Lampert et al., 2003; von Lintig and Vogt, 2004). HPLC analyses were performed on a Hypersil 3 μm column (Knauer, Germany) on a System Gold (Beckman) equipped with a multidiode array (model 166, Beckman) and the Karat software, as previously described (Lampert et al., 2003). The individual retinoids were each determined by their retention times and spectral characteristics as compared to commercially available standards. For quantification of the molar amounts, peak integrals were scaled with defined amounts of reference substances. The reference substances all-*trans* retinyl palmitate and all-*trans*, 13 and 9 retinal were purchased from Sigma. 11 retinal was isolated from dark-adapted bovine eyes. The corresponding retinols and oximes were obtained by the reduction of the retinals with $NaBH_4$ or their reaction with NH_2OH, respectively (von Lintig and Vogt, 2004).

Results

External phenotype of fading vision

The external appearance of the zebrafish mutant *fading vision* (*fdv*) is characterized by a reduced pigmentation of the eyes' RPE and melanocytes in the body (Figs. 1A and B). As development proceeds, the external phenotype becomes progressively stronger, and homozygous *fdv* mutant larvae can be clearly distinguished from wild-type siblings by 5 dpf. At higher magnification, the shape and structure of the melanocytes in *fdv* mutant larvae can be seen to be different from that in the wild-type (Figs. 1C and E). Moreover, melanin is not uniformly distributed within the melanocytes. Occasionally, in some melanocytes, there appears to be no melanin present at all (arrowhead in Fig. 1E). As a result, the appearance of *fdv* larvae is lighter (Fig. 1E) compared to age-matched wild-type larvae (Fig. 1C). Furthermore, the adult fish appear hypopigmented (Figs. 1D and F). In addition to these morphological phenotypes, the positioning of some of the skin melanocytes during development is affected, and several melanocytes can be observed to accumulate beneath the ear in 5-day-old *fdv* mutant embryos (data not shown).

Homozygous fdv larvae have visual deficits not related to axonal misprojections

Subsequent to the identification of *fdv* based on their pigmentation phenotype, a defect in vision was detected in homozygous *fdv* larvae by virtue of a reduced or absent optokinetic response (Neuhauss et al., 1999). In this behavioral assay, larvae view a moving high-contrast grating and respond with stereotypic eye movements. A reduction or an absence of such an optokinetic response is an indication for a compromised visual ability.

A link between the levels of melanin production in the RPE and the extent of misprojecting retinal axons in mammalian species has been recognized for many years. It was suggested that the level of melanin in the RPE roughly correlates with the extent of the ipsilateral projection in the mouse visual system (Balkema and Drager, 1990; LaVail et al., 1978; Rachel et al., 2002). To rule out the possibility that the reduced visual ability in 5-day-old *fdv* larvae is caused by a projection defect in the retinotectal pathway, we injected the lipophilic dye DiI into the eye of 5-day- and 6-day-old larvae (n = 46) and scored the projection of the retinal ganglion cells to the optic tectum. None of the injected larvae showed a defect in the retinotectal projection (data not shown).

Histological analysis of the fdv retina

We examined the eye phenotype in *fdv* mutants at various stages of development by standard histology. By external inspection, homozygous mutant larvae can first be reliably identified at 4 days post fertilization (dpf) due to their body pigmentation phenotype. Hence, we examined sections of mutant and wild-type eyes between 3 and 7 dpf (Fig. 2).

Starting at 3 dpf, when the formation of photoreceptor cell (PRC) outer segments is initiated (Schmitt and Dowling, 1999), the RPE appears less dark than in the wild-type. Closer inspection of the eye phenotype in plastic sections at the light microscopic level revealed a reduced density of melanin granules inside the RPE cells, although individual granules appear similar in coloration to those in the wild-type (Figs. 2A and F).

As development proceeds, the RPE phenotype gets progressively more severe. The density of melanosomes in the RPE of mutant larvae is decreased in comparison to their wild-type siblings. At 5 dpf, melanin clots appear in the

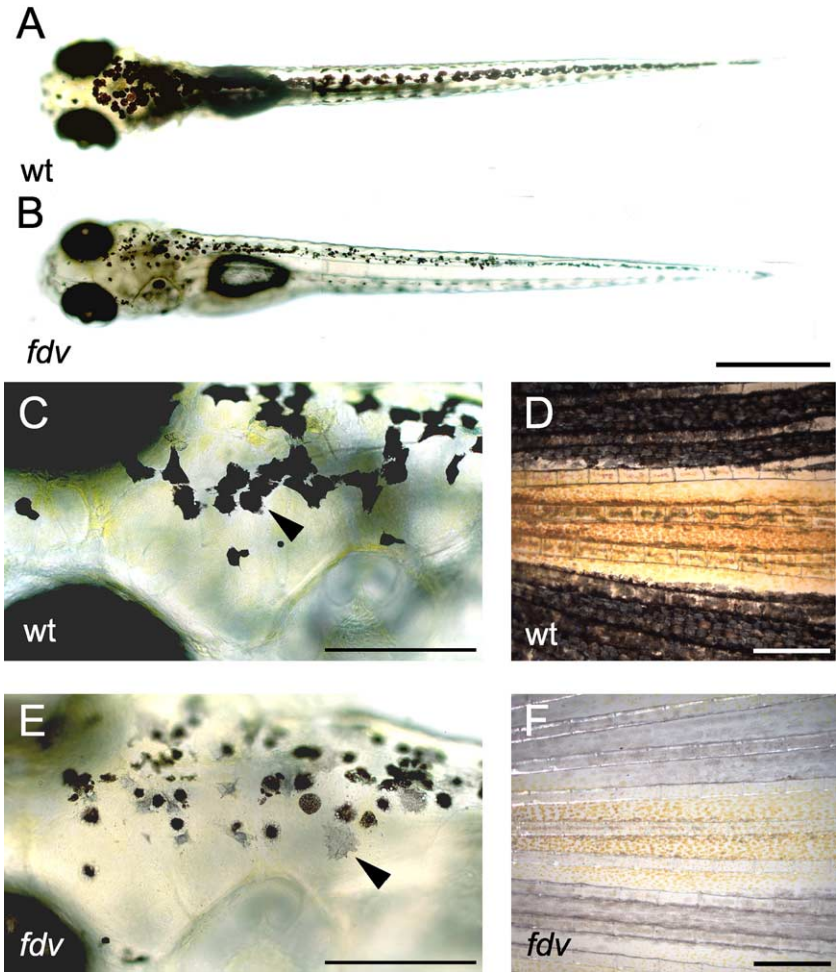

Fig. 1. Body pigmentation of the fading vision mutant. (A) 5-day-old wild-type and (B) *fdv* mutant larva. *fdv* shows lighter body pigmentation compared to the 5-dpf-old wild-type larva. (C, E) Higher magnification reveals that the shape of the pigment cells and the distribution of melanin in the pigment cells are different between (C) 5-dpf-old wild-type larvae and (E) 5-dpf-old *fdv* mutant larvae. (Arrowhead in panels C and E) Some pigment cells appear almost unpigmented. Hypopigmentation is clearly apparent in panel (D) fins of adult wild-type fish compared to (F) homozygous adult *fdv* mutants. Scale bars in panels (A) and (B) are 500 μm. Scale bars in panels (C) and (E) are 200 μm. Scale bars in panels (D) and (F) are 500 μm.

mutant RPE, and its cells begin to fill with large vacuoles, similar to lipid deposits seen in retinas affected by outer retinal degeneration (arrowheads in Fig. 2G). Presumably as a consequence of these changes in the RPE, the outer segments of the PRCs are severely affected. At 5 dpf, they are shorter than in the wild-type (arrowheads in Fig. 2G), and at later stages (7 dpf), the outer segments are even absent in parts of the retina (arrowhead in Fig. 2I). The strongest effects of the mutation are more explicit in the center than in the periphery of the retina. This is probably due to the fact that the phenotype shows an age progression, therefore RPE cells in the center of the retina are more affected than the younger cells in the periphery.

Similar changes in the retina, namely lipid deposits in the RPE and progressive shortening of PRC outer segments, are often associated with apoptosis of outer retina cells. Therefore, we examined the retina at different stages of development with the TUNEL (terminal deoxynucleotidyl transferase-mediated dUTP nick end labeling) assay to specifically label cells undergoing apoptosis. These analyses did not reveal a significant difference in the numbers of apoptotic cells between the mutant and wild-type retinas at any of the developmental stages examined between 5 and 9 dpf (data not shown). This result was consistent with our failure to detect any pyknotic nuclei at both the histological and ultrastructural level of analysis (see Figs. 2 and 3).

Despite their significantly reduced visual ability, homozygous *fdv* individuals can survive to adulthood. However, their survival rate is lower by approximately 40% than that typically observed for wild-type larvae, and homozygous *fdv* larvae can only be raised in isolation, presumably requiring a lack of competition for food with wild-type larvae.

Surprisingly, *fdv* mutant larvae, not only survive, but also show a marked improvement in their visual abilities as adults when assessed by the optomotor response (OMR) (data not shown). On the morphological level, this improvement in vision is mirrored by a partial increase in the length of the PRC outer segments, and microvilli can be seen to extend between the PRC outer segments (arrowheads in

Figs. 2E and J). Moreover, the vacuoles regularly observed in the RPE of *fdv* larvae are virtually absent in the adult, and the overall structure of the RPE is indistinguishable from that of the wild-type (Figs. 2E and J). However, the RPE of adult *fdv* mutants is still lighter pigmented as compared to wild-type. This is probably due to the impaired formation of pigment granules in the RPE (Figs. 2E and J, 3D and H).

The histological analysis indicated that the visual defect in *fdv* likely starts in the RPE then secondarily and progressively affects the PRC outer segments. Although the PRCs and RPE cells are strongly affected, there is no sign of increased cell death, and the defect is restricted to the outer retina, leaving the inner retina completely unaffected at all stages examined (Figs. 2 and 3). The decrease in visual ability can readily be explained by the observed morphological changes of the RPE and the PRC outer segments. Surprisingly, the outer retina recovers during late larval to juvenile stages. Thus, homozygous adult mutants have regained vision to a large extent, as mirrored by the near normal morphology of their outer retinas.

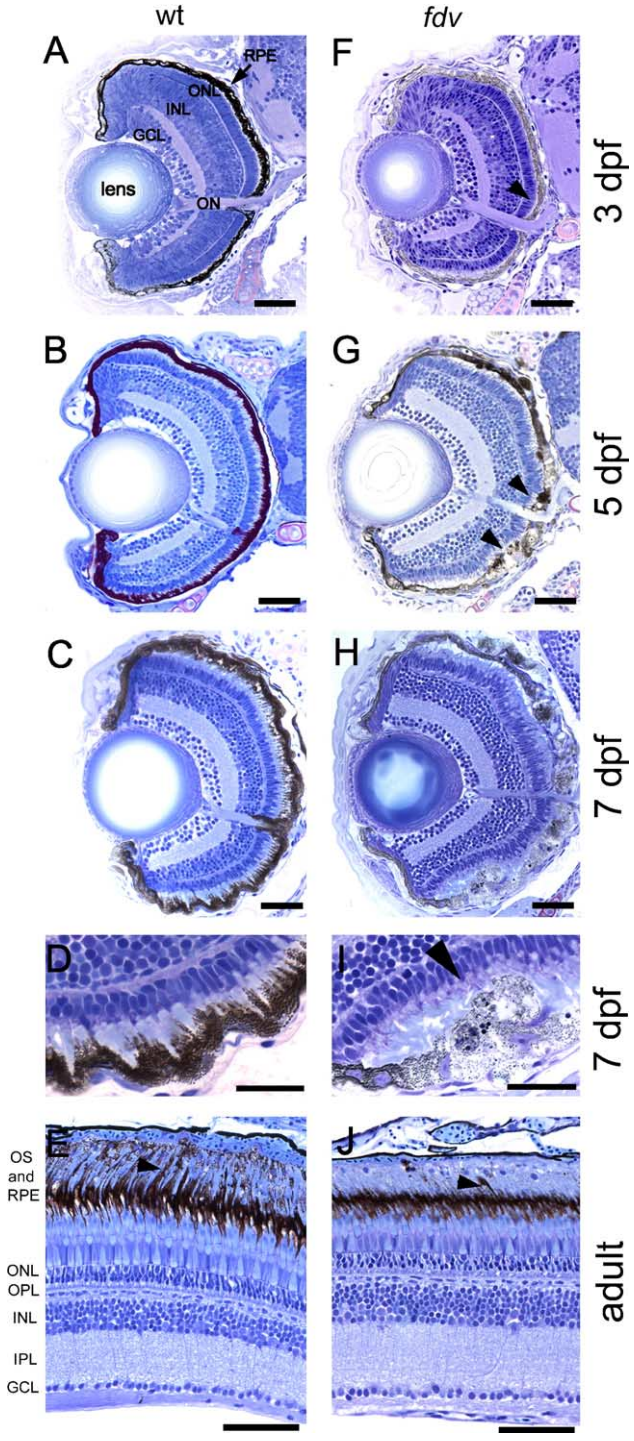

Fig. 2. Histological eye sections at different developmental stages. Comparisons of (A–E) wild-type sections with (F–J) mutant sections show a progressive morphological deterioration in the outer layer of the retina. At 3 dpf, the RPE appears to be lighter pigmented in (F) *fdv* mutants than in (A) wild-type larvae. (B and G) Sections taken from 5-dpf-old larvae show a thickening of the RPE in the mutant larvae, (arrowheads in G) the appearance of pigment clots in the RPE and a reduced length of the outer segments in *fdv* mutants, while the (B) wild-type RPE is densely pigmented and microvilli of the RPE interdigitate with the PRC outer segments. In sections of (H) 7 dpf *fdv* larvae, the RPE is even more severely affected. The RPE cells are lighter pigmented in the mutant, containing pigment clots and no microvilli. PRC outer segments are bent sideways, as can be seen at higher magnification ((D) wild-type and (I) *fdv* mutant) and (arrowhead in panel I) are even absent in some parts of the mutant retina. Surprisingly, a comparison of sections of (J) adult *fdv* mutant and (E) wild-type eyes shows that the RPE and the PRC outer segments have recovered in the mutant, and (arrowheads in panels E and J) microvilli interdigitating in between the outer segments of PRCs can be seen. The inner retina is not affected at any of the developmental stages examined. ON, optic nerve, GCL, ganglion cell layer, IPL, inner plexiform layer, INL, inner nuclear layer, OPL, outer plexiform layer, ONL, outer nuclear layer, OS, outer segments, RPE, retinal pigment epithelium. Scale bars in panels (A–C), (F–H), (E) and (J) are 50 mm. Scale bars in panels (D) and (I) are 20 mm.

Ultrastructural analysis of the fdv retina

In order to examine the morphological defect in the *fdv* mutant at the ultrastructural level, we performed thin-section transmission electron microscopy (TEM) on retinas of different developmental stages.

Small vacuoles can already be observed in the mutant RPE at 3 dpf (Figs. 3A and E). Occasionally, some of these vacuoles contain what appear to be fragments of membranes in a disorganized arrangement. During larval development, these vacuoles become progressively larger (Figs. 3B and F).

In 5-dpf-old *fdv* larvae, the typical microvilli of RPE cells, which at this stage normally interdigitate with the outer segments of the PRCs (arrow Fig. 3B), are rarely detectable. These microvilli are crucial for the function, maintenance and structural stabilization of rod and cone outer segments of PRCs (Marmorstein et al., 1998). Consistent with our histological analysis at the light microscopic level, the PRC outer segments are shorter than in the wild-type and are no longer oriented perpendicular to the eye's surface (Fig. 3F). Moreover, the characteristic palisade-like arrangement of PRC outer segments is

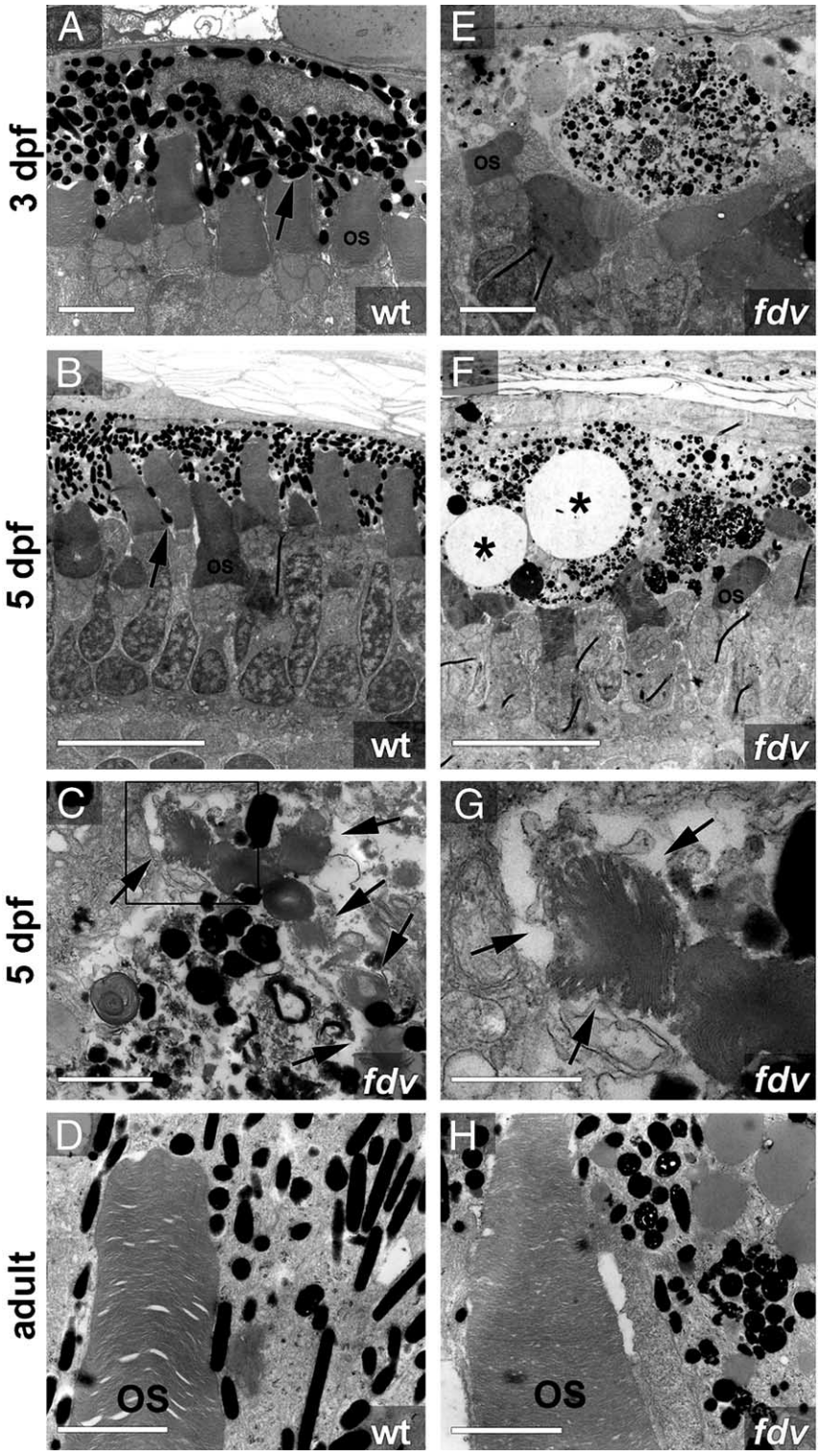

Fig. 3. Transmission electron microscopy from wild-type and *fdv.* Ultrathin sections were taken from (A, E) 3 dpf, (B, C, F, G) 5 dpf and (D, H) adult zebrafish. At larval stages (A–G), PRC outer segments in *fdv* mutants are significantly shorter and the RPE is damaged. In the RPE of *fdv* mutants, vacuoles begin to form at (E) 3 dpf and are prominent at (asterisks in panel F) 5 dpf. Melanin-containing pigment granules are aberrantly shaped. (C and G) Organelles containing detached PRC outer segments can be observed more often within RPE cells of *fdv* mutants than in wild-type larvae. Panel (G) shows a higher magnification of the box depicted in panel (C). The arrows in panels (C) and (G) indicate the undigested stacks of PRC outer segments in the RPE. The microvilli that interdigitate between the PRC outer segments (arrow in panel B) in wild-type larvae are rarely found in larvae of *fdv* mutants. (D, H) In adult *fdv*, the outer segments have recovered, but the melanosomes contain vesicles and some have a fuzzy diffuse shape. OS, outer segments of photoreceptor cells. The thin black lines in panels (B), (E) and (F) are due to preparation artifacts. Scale bars in panels (A) and (E) are 2 μm, in panels (B) and (F) 10 μm, in panel (C) 1 μm, in panel (G) 0,5 μm, in panels (D) and (H) 2 μm.

Table 1
Morphometric analysis of the outer retinal defect

Area covered by	Wild-type larvae (n = 9)	*fdv* larvae (n = 10)	Adult wild-type retinas (n = 4)	Adult *fdv* retinas (n = 4)
RPE	147 (+/−14)	192 (+/−33)	144 (+/−23)	136 (+/−30)
PRC outer segments	245 (+/−34)	83 (+/−15)	234 (+/−25)	189 (+/−72)
PRC nuclei	180 (+/−37)	175 (+/−23)	76 (+/−8)	72 (+/−6)

The point-counting method was used to quantify the area covered by RPE, PRC outer segments and PRC nuclei in larval and adult eyes. Values are given as counted points covered by the respective structure on TEM sections. The area of the bloated RPE is significantly increased in 5-dpf-old mutant larvae compared to wild-type ($P < 0.01$). Outer segment coverage is significantly reduced in 5-dpf-old mutant larvae ($P < 0.001$). However, there is no significant difference in the recovered adult retina.

disrupted, while the somata and the inner segments appear to be normally arranged (Figs. 3B and F).

The cells of the RPE in *fdv* frequently contain vesicle-enclosed PRC outer segments, indicating that the phagocytic activity of the RPE in the mutant is not compromised (Figs. 3C and G). However, we found more outer-segment-containing vesicles in the mutant RPE, suggesting the presence of a defect in the subsequent breakdown of these membrane stacks.

The RPE of 5-day-old mutant larva also contains fewer melanosomes, the vast majority of which are of aberrant shape. In contrast to the characteristic oval melanosomes in the wild-type, mutant melanosomes are uneven and rather spherical in shape (Fig. 3F). Additionally, they regularly contain small and unpigmented areas. Since the black pigment melanin is obviously present in the mutant RPE cells as well as in skin melanocytes, the mutation in *fdv* affects melanin deposition rather than melanin biosynthesis.

The absence of microvilli at the ultrastructural level gives a ready explanation for the disarray of the PRC outer segments. During the outgrowth of the outer segments in development, the microvilli may serve as a scaffold to help in aligning and stabilizing the labile outer segments. Ultrastructural analyses of the adult mutant retina showed a clear improvement in the structure of the PRC outer segments (Figs. 3D and H), which are now enclosed by RPE microvilli, and there is close contact between the outer segments and the RPE. However, the melanosomes in adult *fdv* retinas are still spherically shaped and contain areas lacking pigment, whereas this is rarely seen in the wild-type, indicating that the recovery of the biogenesis of this organelle is not complete.

In order to quantify the changed morphology in the mutant outer retina, we measured the area covered by the RPE and the PRC outer segments on magnification-matched TEM sections. The area covered by PRC nuclei was used as an internal control.

These analyses show that the bloated RPE covers a significantly larger area in mutant larvae as compared to the wild-type ($P < 0.01$; Table 1; see also Figs. 3B and F). Outer segment area is dramatically reduced in *fdv* mutant retinas ($P < 0.001$; Table 1). However, in the adult eye, no significant difference between wild-type and mutant could be found for the areas covered by the PRC outer segments or the RPE, respectively (Table 1). This supports the hypothesis that the outer retinal defect in *fdv* recovers with age.

The fdv mutant is caused by a mutation in the silva gene leading to a truncated protein

To identify the mutation underlying the observed phenotype, we positionally cloned the mutated gene. To do this, the mutant locus was first assigned to a portion of chromosome 11 by pooled segregant genome scan analysis using 192 simple sequence-length polymorphisms (SSLPs). Subsequent segregation analyses of 2446 meioses were performed with three SSLP markers (z3362, z8214, z47584) found to be located in the vicinity of the mutant locus (Fig. 4A). For the

Fig. 4. Identification and structure of *silva*/*fdv*. (A) Mapping of the *fdv* mutation to a genomic interval on linkage group 11. This figure represents a reconstruction of the genomic region surrounding the *fdv* mutation based on information derived from the following maps of the zebrafish genome: the MGH genetic map and the T51 radiation hybrid (RH) map. The genetic positions (cM) of the SSLP markers given in this figure are derived from the MGH genetic map. The values given for the RH position (cR) are taken from the T51 radiation hybrid map (both maps can be found on http://www.zfin.org). The *fdv* mutation was initially placed between the SSLP markers z3362 and z8214 on linkage group 11 by rough mapping. For z3362, 33 recombination events per 1728 meioses were detected, and for the SSLP marker z8214, 28 recombination events per 1728 meioses were detected. The larvae tested for the two markers were taken from different crosses, and the concordance of the numbers of larvae tested is coincidental. Subsequent genetic fine mapping placed *fdv* between the SSLP marker z47584 (14 recombination events per 1728 meioses) and the EST fa95g04 (2 recombination events per 1536 meioses) located at position 358 cR from the top on the T51 radiation hybrid map. The EST fa95g04 corresponds to the zebrafish *timeless* gene. For details on the mapping procedure employed, please refer to the Materials and methods and the Results sections. Screening of the DanioKey and Chori211 BAC libraries using primers designed on the sequence of fa95g04 resulted in the identification of three BACs: CH211-148I19, DKEYP-123E6 and CH211-69H3. While all three BACs were positive when screened for the fa95g04 sequence by PCR analysis, *silva* could only be detected on BAC CH211-148I19. The cross denotes the location of the *fdv* mutation in the genomic region. Arrowheads denote that the direction of the mutation is located as indicated by testing the recombinant larvae. (B) Sequencing of the genomic cds for *silva* revealed a point mutation at nucleotide position 1468, leading to a premature stop codon. The predicted truncated protein lacks the proteolytic cleavage site, the transmembrane domain and the AP3 binding motif. (SP, red) Signaling peptide, (PKD, blue) polycystic kidney disease domain, and (TM, green) transmembrane domain. (C) Protein sequence of zebrafish Silv. (C, black) The low complexity region containing the repeats is underlined. (SP, red) Signaling peptide, (PKD, blue) polycystic kidney disease domain, (TM, green) transmembrane domain. The mutated amino acid is indicated by a red asterisk.

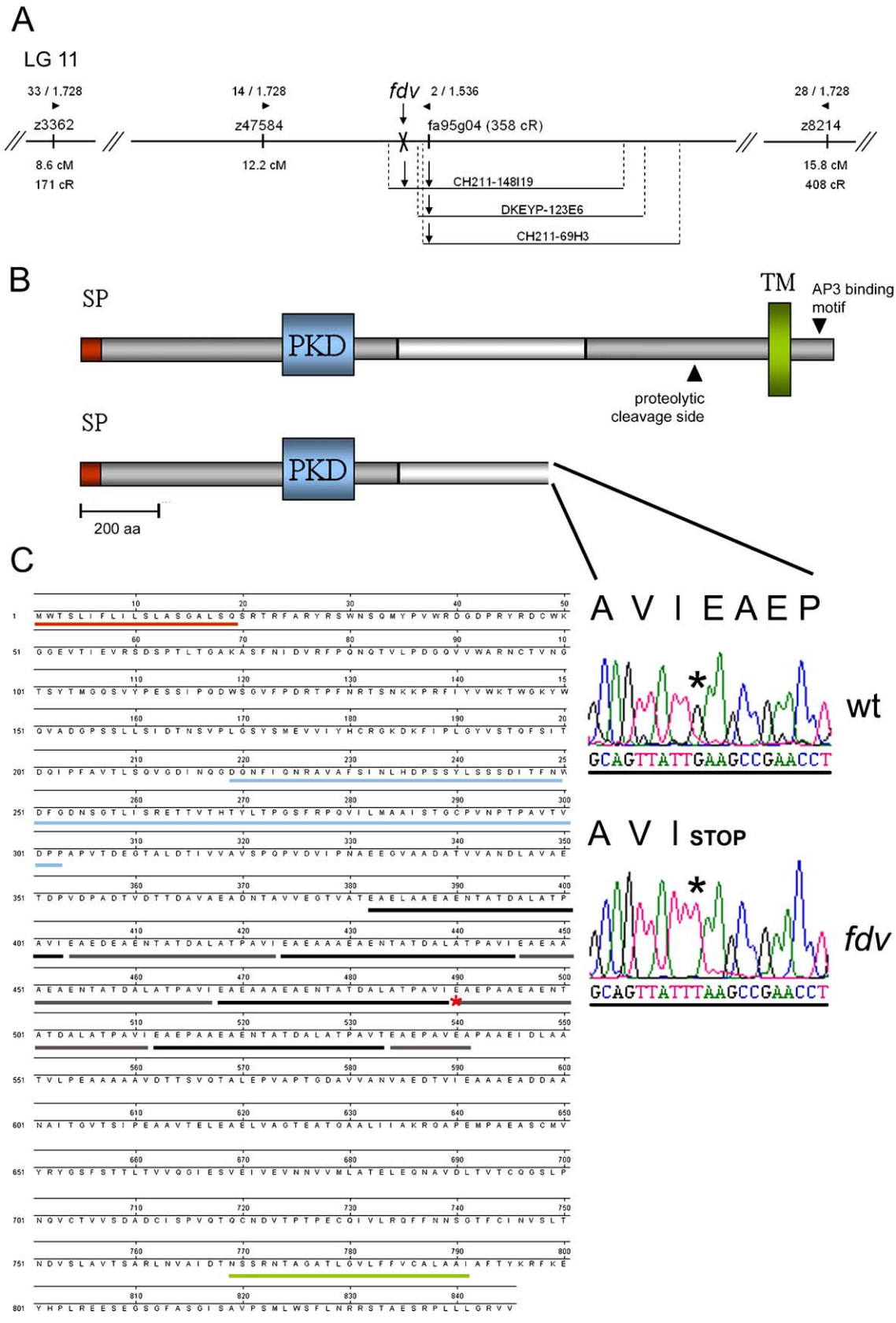
A
LG 11
33 / 1.728
14 / 1.728
fdv 2 / 1.536
28 / 1.728
z3362
z47584
fa95g04 (358 cR)
z8214
8.6 cM
171 cR
12.2 cM
15.8 cM
408 cR
CH211-148I19
DKEYP-123E6
CH211-69H3
B
SP
PKD
TM
AP3 binding motif
proteolytic cleavage side
SP
PKD
200 aa
C
A V I E A E P
wt
GCAGTTATTGAAGCCGAACCT
A V I STOP
fdv
GCAGTTATTTAAGCCGAACCT

subsequent fine mapping, we identified single nucleotide polymorphisms (SNPs) from expressed sequence tag (EST) sequences located in this genomic region as identified from the T51 radiation hybrid map (Geisler et al., 1999). PCR products of 17 ESTs were analyzed for single-strand conformation polymorphisms (SSCPs). Following the SNP analysis of embryos recombinant for markers z3362, z47584 and z8214, the EST fa95g04 was identified as being the EST closest to the mutant locus (2 recombination events out of 1536 meioses), with an estimated genetic distance of approximately 0.1 cM (estimated to correspond to approximately 74 kb in zebrafish (Shimoda et al., 1999)) (Fig. 4A).

In order to further narrow down the genomic interval, fa95g04 was used to screen two different bacterial artificial chromosome (BAC) zebrafish genomic libraries, Chori211 and DanioKey (Geisler, 2002). A total of eight BAC clones were identified to be positive for the fa95g04 sequence used to screen the libraries. By mapping the BAC end sequences on the T51 radiation hybrid panel of the zebrafish genome, three BACs, CH211-148I19, DKEYP-123E6 and CH211-69H3, were verified to be located in the same genomic interval as the mutation (Fig. 4A). A screen of the first fingerprint contigs (fpc) database of the Sanger Institute (http://www.sanger.ac.uk/Projects/D_rerio/WebFPC/zebra/small.shtml) identified a contig containing these three BACs.

In parallel, the end sequences of the identified BAC clones were used for a database screen of the first zebrafish genome assembly of the Sanger Institute (ASSEMBLY Zv1/06, www.sanger.ac.uk). These sequences all fell onto a genomic assembly of approximately 275 kb. On this assembly, we also found fa95g04, the closest EST identified by SSCP mapping, giving independent confirmation of the candidate region. Within this 275 kb interval, 5 transcription units were predicted by GENSCAN (http://genes.mit.edu/GENSCAN.html; Burge and Karlin, 1997), which showed homologies to five genes (*tubulin beta 2*, *timeless*, *silver*, *MMP8* and *copine8*). Comparing the putative functions of these genes with the *fdv* phenotype, we selected the *silver* (*silv*) gene as the most likely candidate. Since we identified a second paralogue of this gene in zebrafish, we named this gene *silver a* (*silva*). We tested the hypothesis of *silva* being the mutated gene in *fdv* mutants by cloning and sequencing of the zebrafish *silva* cDNA from reverse transcribed (RT-PCR) total cDNA obtained from wild-type and *fdv* mutant larval and adult tissue. The primers for the amplification of the *silva* cds were designed based on the sequences of ESTs fj24g11, fj03d05 and fc11g11 (Clark et al., 2001), which were obtained by BLAST searches using the mouse and human Silv protein sequences. The coding sequence (cds) of the zebrafish *silva* gene is 2538 bp long, coding for a protein of 845 amino acid residues with a predicted molecular mass of approximately 89 kDa.

Comparison of the wild-type and *fdv silva* sequences identified a single base pair exchange from G to T at position 1468 in the *fdv silva* sequence, resulting in a predicted premature stop codon at amino acid residue position 490 (Fig. 4B). The predicted truncated mutant protein lacks the terminal 355 amino acid residues, including one domain and two motives important for localization and function of the protein. These include the transmembrane domain, the predicted proteolytic cleavage site and the AP3 binding motif (Le Borgne et al., 2001) (Fig. 4B).

Alignment of the human, mouse and zebrafish *silva* genes revealed an interesting case of divergent sequence evolution between different protein domains. The domain prediction by SMART (Simple modular architecture tool, http://smart.embl-heidelberg.de/) resulted in three domains for zebrafish Silva: a signaling peptide comprising the first 19 amino acids, a PKD (polycystic kidney disease) domain spanning amino acids 219 to 303 and a transmembrane domain from amino acid 769 to 791 (Fig. 4B). Moreover, the Silva protein contains a proteolytic cleavage site at positions 632 to 640 and an AP3 binding motif in the

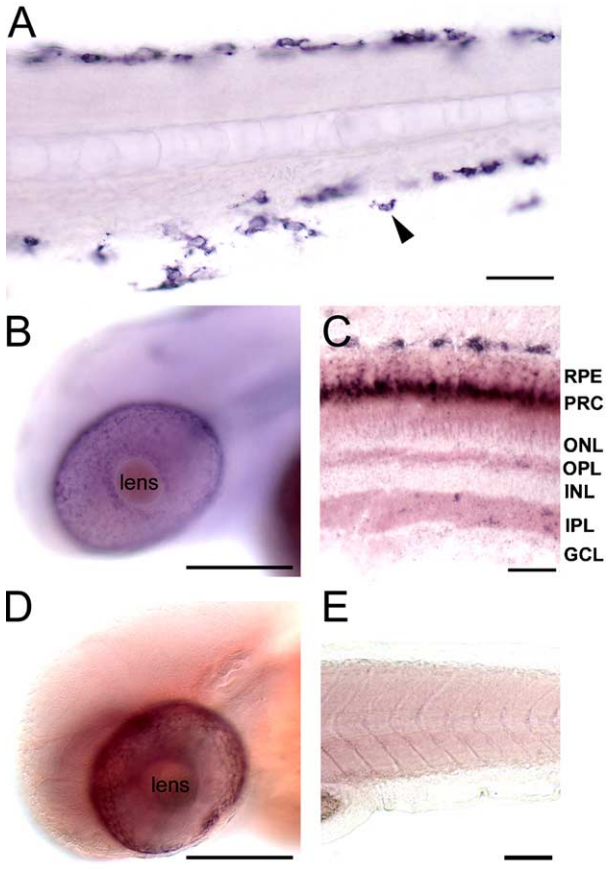

Fig. 5. Spatio-temporal expression pattern of *silva* and *silvb*. Expression analyses in 2-day-old wild-type larva. (A and B) *silva* is expressed in (arrowheads in A) melanocytes and (B) the RPE of the eye. (C) On adult sections, the *silva* transcript is confined to cells of the RPE and to the melanocytes located behind the eye. (D and E) *silvb* expression is restricted to RPE cells. RPE, retinal pigment epithelium, PRC, photoreceptor outer segments, ONL, outer nuclear layer, OPL, outer plexiform layer, INL, inner nuclear layer, IPL, inner plexiform layer, GCL, ganglion cell layer. Scale bar in panel A is 50 μm, in panels B and D 100 μm, in panel C 20 μm and in panel E 50 μm.

cytoplasmic part of the protein, analogous to the mouse and human proteins (Berson et al., 2003; Raposo et al., 2003). The overall domain structure predicted for the zebrafish Silva protein is homologous to the domain structure found in the human and mouse Silv proteins. A notable exception is the low complexity region in the center of the protein, spanning amino acids 382 to 549 in zebrafish Silva (Fig. 4C). In this region, a repetitive sequence of about 22 amino acids in length is repeated 7.4 times. This repetitive element shows sequence similarity to vertebrate repetitive elements pTAR5 and mer22. Intriguingly, the mouse and the human Silv proteins contain only 2 and 3 repetitive elements, respectively, but these show little sequence homology to the repetitive element encoded in the zebrafish gene, and the low complexity region of the *silva* gene is longer than in the mammalian genes.

In order to examine whether the expression profile of *silva* is consistent with the mutant phenotype, we performed mRNA in situ hybridization expression analyses at different developmental stages. By using antibodies to digoxigenin-labeled RNA probes, expression could be detected in the cells of the RPE and in skin melanocytes of developing larvae (Figs. 5A and B). This expression persists into adulthood and is restricted to melanogenic cells at all times (Fig. 5C). This expression pattern provided support for the hypothesis that *silva*, a true zebrafish orthologue, and its expression in cells affected by the *fdv* mutation substantiate our inference that *fdv* represents a mutation in *silva*.

In contrast to mammals, we isolated a second orthologue in zebrafish, named *silver b* (*silvb*). The sequencing of the zebrafish *silvb* resulted in a 1851 base pair open reading frame, coding for a protein of 617 amino acids. *silvb* expression analysis revealed exclusive expression in RPE cells, in contrast to *silva*, which is also expressed in melanocytes (Figs. 5D and E).

fdv can be phenocopied by silva knock-down

The genomic localization, the induced STOP codon, the nature of the *silva* gene and the spatial and temporal expression pattern of the *silva* gene provides strong evidence that this mutation causes the *fdv* phenotype. In order to obtain additional proof that a mutation in *silva* is causative of the *fdv* phenotype, we attempted to create

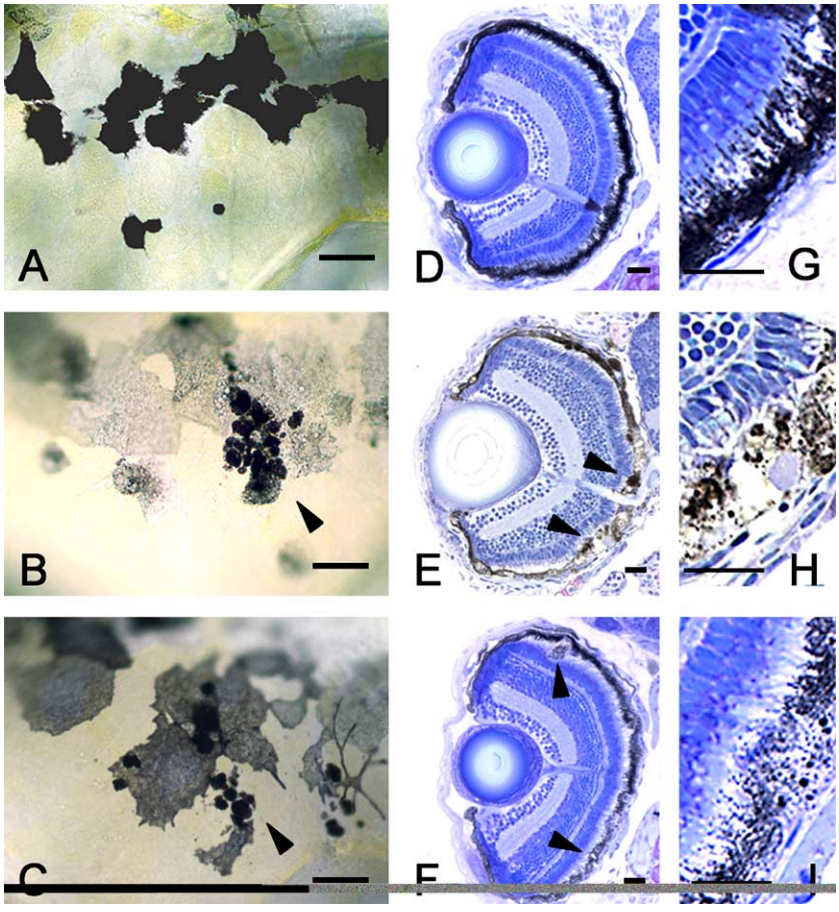

Fig. 6. Phenocopy of *fdv* by *silva* knock-down. (C, F, I) Morpholino-oligonucleotide-injected 5-day-old larvae show the same phenotype as (B, E, H) 5-day-old *fdv* mutant larvae. Compared to the (A, D, G) wild-type, the melanocytes are lighter and contain pigment clots (arrowheads in panels C and F). In the sections taken from (arrowheads in panel F) larvae after morpholino injection, some RPE cells are bloated and contain vacuoles as can be seen in (arrowheads in panel E) *fdv* mutant larvae. Scale bars in panels A–C are 20 μm, in panels D–F 100 μm and in panels G–I 50 μm.

a phenocopy of the mutant by a specific gene knock-down. Toward this goal, we designed antisense morpholino oligonucleotides targeted against the translational start region to block translation of *silva*. Injection of these antisense nucleotides into embryos at the one cell stage leads to lighter body pigmentation and pigment granules of RPE cells and melanocytes that are clumped together as seen in 5-dpf-old *fdv* mutant larvae (Fig. 6C). As described for the *fdv* mutants, morpholino-injected larvae were clearly distinguishable from wild-type larvae at 5 dpf.

Histological eye sections taken from 5-day-old morpholino-injected embryos confirmed the hypopigmentation of the RPE (Fig. 6F). Moreover, the sections of these larvae revealed the bloated appearance of individual cells in the RPE, and the disorganization of the PRC outer segments underneath bloated RPE cells (arrowhead in Fig. 6F), as seen in the *fdv* mutant larvae. The characteristic accumulation of melanocytes under the ear of 5-day-old *fdv* mutant larvae was also observed in age-matched morpholino-injected embryos (data not shown). The injection of a control morpholino led to no visible phenotypes. Thus, the injection of a morpholino antisense nucleotide leads to a close phenocopy of the *fdv* mutant, confirming the molecular defect of the mutant. It should however be noted that, even at the highest amount injected, the knock-down phenotype was less severe than the mutation. This is possibly due to the progressive dilution of the morpholino molecules at later stages of embryonic development, particularly since eye growth is substantial during early larval stages.

fdv is affected in visual pigment regeneration

The main functional involvement of the RPE in vision is the recycling of visual pigment. In PRC outer segments, 11 retinal isomerizes to all-*trans* retinal upon absorption of light. The subsequent reisomerization takes place to a large extent in the RPE in a process called the visual cycle (Rando, 2001). Since vision is affected in *fdv* and the RPE is filled with vesicles of unknown content, we determined the relative amounts of visual cycle intermediates in the mutant larval and adult retinas.

For this purpose, the heads of dark-adapted larvae were dissected under dim red light. Retinoids were extracted and subjected to HPLC analyses as previously described (Lampert et al., 2003; von Lintig and Vogt, 2000). In the larval eyes, the major retinoids are retinyl esters and 11 retinal, with traces of all-*trans* retinal (Fig. 7A). The total retinoid content of the mutant and wild-type eyes from 7-day-old larvae is comparable; for the wild-type: 9.36 pmol, and for *fdv*: 8.78 pmol. However,

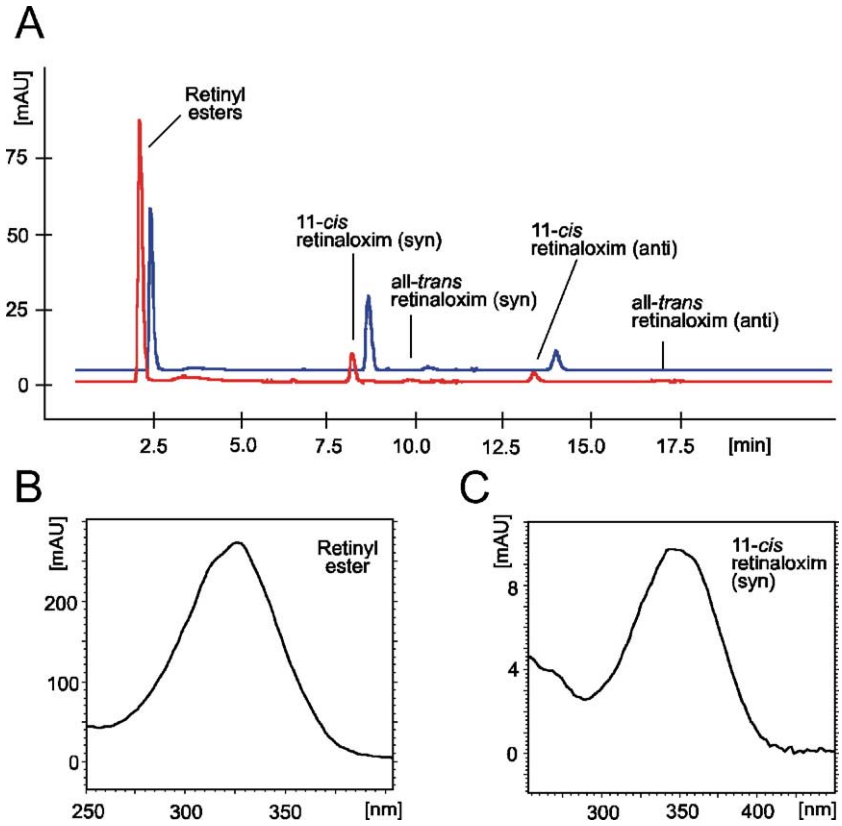

Fig. 7. HPLC profiles at 360 nm of the extracts of heads of 7 dpf *fdv* and wild-type larvae. Retinoids from the eyes of *fdv* and wild-type siblings (n = 63 each) were extracted as described in the Materials and methods. The retinoids were subjected to HPLC analyses. (A) HPLC profile at 360 nm of dark-adapted *fdv* (red) and wild-type larvae (blue). The composition of the individual retinoids is indicated. (B) Absorption spectra of retinyl ester and (C) 11 retinal oxime (syn).

Table 2
Biochemical analyses of the visual cycle of *fdv* mutant larvae and adults

Retinoids [pmol/eye pair]	*fdv* larvae	Wild-type larvae	*fdv* adult	Wild-type adult
Retinyl esters	7.05	6.61	801	742
11 retinal	1.26	2.44	92	229
Ratio [retinyl esters/11 retinal]	5.59	2.7	8.7	3.2
Total retinoids	8.78	9.36	893	971

Composition and molar amounts of the individual retinoids of the eyes of dark-adapted 7-dpf-old larvae and adult eyes as compared to wild-type controls. The values give the means of two independent experiments.

the ratio of retinyl esters to 11 retinal is lower in wild-type larvae compared to *fdv* mutant larvae (see Table 2), reflecting a reduction of 11 retinal in mutant larvae. We then analyzed the retinoid composition in dark-adapted eyes of age-matched adult *fdv* and wild-type control zebrafish. Again, we found a reduction in the amounts of 11 retinal in *fdv* as compared to controls (see Table 2). The retinyl ester content was elevated in *fdv* as compared to control zebrafish. Hence, the visual cycle is partially blocked with the intermediate product retinyl ester accumulating at the expense of the regenerated visual chromophore 11 retinal.

Discussion

The retinal pigment epithelium (RPE) plays an essential role in the maintenance of photoreceptors, phagocytosing shed outer segments and regenerating the photopigment in a process called the visual cycle (Bok, 1993). The RPE synthesizes the interphotoreceptor extracellular matrix and provides for the selective shuttling of ions and metabolites (Schraermeyer and Heimann, 1999). Additionally, the RPE reduces backscattering of light in the eye by means of melanin containing organelles (melanosomes). These melanosomes also serve to reduce and protect RPE cells from oxidative damage by radicals arising during phagocytosis and photopigment recycling (McBee et al., 2001). Additionally, the RPE plays a crucial role in the development and maintenance of the retina by secreting a number of growth factors, providing a pool of anti-oxidants, as well as structurally stabilizing the cone and rod outer segments (Hollyfield, 1999; Steinberg, 1985). There is good evidence that an altered RPE function may cause or contribute to many inherited or acquired retinal degenerations (Michaelides et al., 2003).

Here, we describe the characterization and first molecular cloning of a zebrafish melanosome biogenesis mutant, *fading vision* (*fdv*). This mutant is primarily affected in melanosome biogenesis, leading to hypopigmentation of melanogenic cells of the RPE and skin melanocytes, ultimately resulting in an impairment of visual function in 5-day-old zebrafish larvae. This reduction in visual ability is mirrored on the cellular level in the strongly affected outer retina, with photoreceptors showing fewer, shorter and misaligned outer segments. Surprisingly, these defects ameliorate as development proceeds. Mutant adult retinas still display shorter PRC outer segments and aberrant melanosomes, but the outer segments are arranged in the normal palisade-like fashion. This gradual recovery is accompanied by a partial recovery of visual function (data not shown). Ultrastructural analysis of RPE cells and melanocytes reveals fewer melanosomes, which are of aberrant shape and uneven color in the RPE and melanocytes, indicative of a defect in intraorganelle melanin organization rather than melanin synthesis. Recently, we identified a second *silvb* gene in zebrafish, which might have a compensatory effect in the *fdv* mutants. The duplication of the *silv* gene in zebrafish is probably due to a genome duplication that took place in the lineage after the divergence of ray- and lobe-finned fishes (Gates et al., 1999; Postlethwait et al., 2000). The *silvb* gene displays a comparable homology on the protein level to the human orthologue as *silva*.

The proposed role of Silva in melanosome biogenesis and function is substantiated by the pigmentation defect in *silver* mice (Dunn, 1930). In the *silver* mutant, the Silv protein is truncated, indicating that an intact cytoplasmic domain is needed for its function (Kwon et al., 1991; Martinez-Esparza et al., 1999). However, the gene product has not been implicated in visual system development.

We have identified the molecular defect underlying the *fdv* phenotype by mapping the mutation to a genomic interval spanning 3.6 cM. Further fine mapping of the mutation leads to the identification of a marker, EST fa95g04, located at a distance of approximately 0.1 cM (corresponding to an estimated 74 kb in the zebrafish genome (Shimoda et al., 1999) south of the mutation. A database search resulted in the identification of a candidate gene, *silva*, which is located approximately 0.1 cM north of this marker and thus at the position of the *fdv* mutation. As we were able to identify a plausible candidate gene in very close proximity of the EST fa95g04, we did not close in on the mutation from the north of the interval and focused on the analysis of the candidate gene *silva*. Sequencing of *silva* from independent PCR reaction of wild-type and *fdv* mutant larvae revealed a point mutation leading to a premature stop codon in the *silva* (also known as pmel17, gp100 and ME20) gene. The resulting phenotype is consistent with the expression pattern of this gene, in that exclusively cells expressing the gene are affected in the mutant. In order to provide further evidence that the *silva* gene is the mutated gene in *fdv*, we performed antisense morpholino oligonucleotide injections. A knock-down of the Silva protein leads to the same loss-of-function phenotype as the genetic mutation. The specificity of the morpholino used in this study for *silva* was assured by designing it to target a region of *silva*, which differs from the *silvb* sequence in 14 of the 25 bases (usually a difference of 5 base pairs is sufficient to avoid binding of control mismatch morpholinos (Corey and Abrams, 2001)).

silva is exclusively expressed in melanogenic cells. The melanosomes in these cells are characterized by proteineous fibers in their lumen, thought to be involved in sequestering melanin. Silv has been shown to be required for the formation of these fibers. The protein localizes to the fibrils, and its ectopic expression in non-pigmented cells is sufficient to induce the formation of premelanosome-like fibers in these cells (Berson et al., 2001). This type I integral membrane protein polymerizes into amyloid-like fibrils. Intraluminal assembly of Silv requires proteolysis by a furin-type proprotein convertase, paralleling amylogenic pathologies (Berson et al., 2003). Proteolytic processing yields a smaller membrane bound fragment of unknown function (Mβ) and a larger cytosolic fragment (Mα) capable of forming fibrils. This mechanism shows a striking parallel between the physiological formation of fibers in melanogenesis and the pathogenic formation of amyloid fibers (Huff et al., 2003).

The defect in melanosome shape and intralumenal distribution of melanin in the *fdv* mutant can plausibly be explained by a defect in the amyloid-like fiber network of melanosomes. The *fdv* mutation is predicted to yield a truncated protein lacking the transmembrane domain, the proteolytic cleavage site and the AP3 binding motif.

Given its molecular nature, it was rather surprising that the larval *fdv* mutant was also found to be defective in vision (Neuhauss et al., 1999). Our morphological analysis demonstrating highly abnormal PRC outer segments provides a likely explanation for the visual function defect. In addition to the morphological alterations, we also found a partial block in the visual cycle, involved in the recycling of the visual pigment by biochemical retinoid analysis. This is a novel and unexpected finding, being the first case of a melanosome organelle biogenesis mutation affecting the visual system on the level of defects seen in morphology, biochemistry and function.

Since *silva* is not expressed in photoreceptors, the deficit must be attributed to a disruption of the interaction between photoreceptors and the RPE. Particularly, the observed absence of RPE microvilli suggests a scenario whereby the outgrowth of PRC outer segments is guided by these finger-like structures. As PRCs form and extend outer segments, RPE cells respond by extending long microvilli into the subretinal space encompassing the outer segments (Marmorstein et al., 1998). In early larval stages, the outer segments are still small compared to the adult retina, but they are already ensheated by these RPE microvilli. The observed lack of a proper palisade-like arrangement of the outer segments is consistent with a role for microvilli in providing both mechanical stabilization, as well as supporting directed outgrowth. The involvement of secreted factors from the RPE is likely since trophic support of photoreceptors by RPE-secreted growth factors has been reported (McBee et al., 2001).

The partial block of the visual cycle could also be attributed to the absence of microvilli or a metabolic dysregulation in RPE cells. Intermediate products of the visual cycle are shuttled between the photoreceptor outer segments and the RPE by specific retinoid-binding proteins and a highly specialized extracellular matrix (McBee et al., 2001). Since physical contact is needed for efficient execution of the visual cycle, a reduced physical contact might be a cause for the observed defect in visual pigment regeneration. However, the recovery of cell contact in the adult outer retina without concomitant recovery of the visual cycle argues against physical contact being the sole contributing factor. Since the cellular morphology of RPE cells is severely disrupted, another concurring factor could be a general metabolic derailment. In the *fdv* mutant, RPE cells are presumably damaged due to a lack of detoxification of melanin intermediates by intralumenal fibers, consistent with the proposed role of melanosomes in detoxification (Kobayashi et al., 1994; McBee et al., 2001).

This is the first report of the molecular cloning of a zebrafish melanosome biogenesis mutant. The zebrafish offers a number of advantages for the study of organelle biogenesis, especially due to the availability of mutants. Since zebrafish larvae develop externally and are transparent, pigment cells can easily be imaged even at the subcellular level in the intact animal. For instance, the *silv* gene has been nearly exclusively studied in cell culture, preventing our reported cellular interaction studies between RPE and photoreceptors to be observed. Since zebrafish larvae are behaviorally highly visual animals (Bilotta and Saszik, 2001; Neuhauss, 2003), we have established a surprising link between vision and organelle biosynthesis.

The near future will likely see an increasing number of relevant mutant strains being isolated and molecularly characterized, allowing a detailed genetic and functional dissection of organelle biosynthesis. Mutant strains such as *fdv* will become important tools to further probe the intricate interaction between photoreceptors and the pigment epithelium of the eye.

Acknowledgments

The authors like to thank Brigitte Sailer and Ursula Müller, Beate Zieser and David Belet for skilled technical assistance. We also like to thank Christa Neumeyer for providing equipment for OMR measurements of zebrafish. The authors also thank Drs. Martin Schwab, Lukas Sommer, Dana Dodd and Ralf Dahm for fruitful discussions and critical reading of the manuscript and Dr. Martin Schwab for financial support. We thank Dr. Victor Canfield for suggesting the duplicated *pmel17* gene to us.

This work was supported by the Swiss National Science Foundation (SNF) and ETH internal grants. S.C.F.N. is a SNF Förderprofessor; R.G was supported by the German Human Genome Project (DHGP grant 01 KW9919).

This work was partially supported by the European Commission as part of the ZF-MODELS Integrated

Project in the 6th Framework Programme (Contract No. LSHG-CT-2003-503496).

References

Balkema, G.W., Drager, U.C., 1990. Origins of uncrossed retinofugal projections in normal and hypopigmented mice. Vis. Neurosci. 4, 595–604.

Berson, J.F., Harper, D.C., Tenza, D., Raposo, G., Marks, M.S., 2001. Pmel17 initiates premelanosome morphogenesis within multivesicular bodies. Mol. Biol. Cell 12, 3451–3464.

Berson, J.F., Theos, A.C., Harper, D.C., Tenza, D., Raposo, G., Marks, M.S., 2003. Proprotein convertase cleavage liberates a fibrillogenic fragment of a resident glycoprotein to initiate melanosome biogenesis. J. Cell Biol. 161, 521–533.

Bilotta, J., Saszik, S., 2001. The zebrafish as a model visual system. Int. J. Dev. Neurosci. 19, 621–629.

Bok, D., 1985. Retinal photoreceptor–pigment epithelium interactions, Friedenwald lecture. Invest. Ophthalmol. Visual Sci. 26, 1659–1694.

Bok, D., 1993. The retinal pigment epithelium: a versatile partner in vision. J. Cell Sci., Suppl. 17, 189–195.

Brand, M.G.M, Nüsslein-Volhard, C.H., 2002. Keeping and raising zebrafish. In: Nusslein-Volhard, C., Dahm, R. (Eds.), Zebrafish, Practical Approach Series. Oxford Univ. Press, pp. 7–37.

Burge, C., Karlin, S., 1997. Prediction of complete gene structures in human genomic DNA. J. Mol. Biol. 268, 78–94.

Clark, M.D., Hennig, S., Herwig, R., Clifton, S.W., Marra, M.A., Lehrach, H., Johnson, S.L., Group t, W., 2001. An oligonucleotide fingerprint normalized and expressed sequence tag characterized zebrafish cDNA library. Genome Res. 11, 1594–1602.

Corey, D.R., Abrams, J.M., 2001. Morpholino antisense oligonucleotides: tools for investigating vertebrate development. Genome Biol. 2, 1015.1–1015.3.

Dunn, L.C., Thigpen, L.W., 1930. The silver mouse: a recessive color variation. J. Hered., 495–498.

Gates, M.A., Kim, L., Egan, E.S., Cardozo, T., Sirotkin, H.I., Dougan, S.T., Lashkari, D., Abagyan, R., Schier, A.F., Talbot, W.S., 1999. A genetic linkage map for zebrafish: comparative analysis and localization of genes and expressed sequences. Genome Res. 9, 334–347.

Geisler, R., 2002. Mapping and cloning. In: Nusslein-Volhard, C., Dahm, R. (Eds.), Zebrafish, Practical Approach Series. Oxford Univ. Press, pp. 175–212.

Geisler, R., Rauch, G.J., Baier, H., van Bebber, F., Brobeta, L., Dekens, M.P., Finger, K., Fricke, C., Gates, M.A., Geiger, H., Geiger-Rudolph, S., Gilmour, D., Glaser, S., Gnugge, L., Habeck, H., Hingst, K., Holley, S., Keenan, J., Kirn, A., Knaut, H., Lashkari, D., Maderspacher, F., Martyn, U., Neuhauss, S., Haffter, P., et al., 1999. A radiation hybrid map of the zebrafish genome. Nat. Genet. 23, 86–89.

Haffter, P., Granato, M., Brand, M., Mullins, M.C., Hammerschmidt, M., Kane, D.A., Odenthal, J., van Eeden, F.J., Jiang, Y.J., Heisenberg, C.P., Kelsh, R.N., Furutani-Seiki, M., Vogelsang, E., Beuchle, D., Schach, U., Fabian, C., Nusslein-Volhard, C., 1996. The identification of genes with unique and essential functions in the development of the zebrafish, *Danio rerio*. Development 123, 1–36.

Hollyfield, J.G., 1999. Hyaluronan and the functional organization of the interphotoreceptor matrix. Invest. Ophthalmol. Visual Sci. 40, 2767–2769.

Huff, M.E., Balch, W.E., Kelly, J.W., 2003. Pathological and functional amyloid formation orchestrated by the secretory pathway. Curr. Opin. Struct. Biol. 13, 674–682.

Hukriede, N., Fisher, D., Epstein, J., Joly, L., Tellis, P., Zhou, Y., Barbazuk, B., Cox, K., Fenton-Noriega, L., Hersey, C., Miles, J., Sheng, X., Song, A., Waterman, R., Johnson, S.L., Dawid, I.B., Chevrette, M., Zon, L.I., McPherson, J., Ekker, M., 2001. The LN54 radiation hybrid map of zebrafish expressed sequences. Genome Res. 11, 2127–2132.

Kelly, J.W., Balch, W.E., 2003. Amyloid as a natural product. J. Cell Biol. 161, 461–462.

Kelsh, R.N., Brand, M., Jiang, Y.J., Heisenberg, C.P., Lin, S., Haffter, P., Odenthal, J., Mullins, M.C., van Eeden, F.J., Furutani-Seiki, M., Granato, M., Hammerschmidt, M., Kane, D.A., Warga, R.M., Beuchle, D., Vogelsang, L., Nusslein-Volhard, C., 1996. Zebrafish pigmentation mutations and the processes of neural crest development. Development 123, 369–389.

Kimmel, C.B., Ballard, W.W., Kimmel, S.R., Ullmann, B., Schilling, T.F., 1995. Stages of embryonic development of the zebrafish. Dev. Dyn. 203, 253–310.

Kobayashi, T., Urabe, K., Orlow, S.J., Higashi, K., Imokawa, G., Kwon, B.S., Potterf, B., Hearing, V.J., 1994. The Pmel 17/silver locus protein. Characterization and investigation of its melanogenic function. J. Biol. Chem. 269, 29198–29205.

Kwon, B.S., Chintamaneni, C., Kozak, C.A., Copeland, N.G., Gilbert, D.J., Jenkins, N., Barton, D., Francke, U., Kobayashi, Y., Kim, K.K., 1991. A melanocyte-specific gene, Pmel 17, maps near the silver coat color locus on mouse chromosome 10 and is in a syntenic region on human chromosome 12. Proc. Natl. Acad. Sci. U. S. A. 88, 9228–9232.

Lampert, J.M., Holzschuh, J., Hessel, S., Driever, W., Vogt, K., von Lintig, J., 2003. Provitamin A conversion to retinal via the beta,beta-carotene-15,15′-oxygenase (bcox) is essential for pattern formation and differentiation during zebrafish embryogenesis. Development 130, 2173–2186.

LaVail, J.H., Nixon, R.A., Sidman, R.L., 1978. Genetic control of retinal ganglion cell projections. J. Comp. Neurol. 182, 399–421.

Le Borgne, R., Planque, N., Martin, P., Dewitte, F., Saule, S., Hoflack, B., 2001. The AP-3-dependent targeting of the melanosomal glycoprotein QNR-71 requires a di-leucine-based sorting signal. J. Cell Sci. 114, 2831–2841.

Marmorstein, A.D., Finnemann, S.C., Bonilha, V.L., Rodriguez-Boulan, E., 1998. Morphogenesis of the retinal pigment epithelium: toward understanding retinal degenerative diseases. Ann. N. Y. Acad. Sci. 857, 1–12.

Martinez-Esparza, M., Jimenez-Cervantes, C., Bennett, D.C., Lozano, J.A., Solano, F., Garcia-Borron, J.C., 1999. The mouse silver locus encodes a single transcript truncated by the silver mutation. Mamm. Genome 10, 1168–1171.

McBee, J.K., Palczewski, K., Baehr, W., Pepperberg, D.R., 2001. Confronting complexity: the interlink of phototransduction and retinoid metabolism in the vertebrate retina. Prog. Retinal Eye Res. 20, 469–529.

Michaelides, M., Hunt, D.M., Moore, A.T., 2003. The genetics of inherited macular dystrophies. J. Med. Genet. 40, 641–650.

Neuhauss, S.C., 2003. Behavioral genetic approaches to visual system development and function in zebrafish. J. Neurobiol. 54, 148–160.

Neuhauss, S.C., Biehlmaier, O., Seeliger, M.W., Das, T., Kohler, K., Harris, W.A., Baier, H., 1999. Genetic disorders of vision revealed by a behavioral screen of 400 essential loci in zebrafish. J. Neurosci. 19, 8603–8615.

Pacione, L.R., Szego, M.J., Ikeda, S., Nishina, P.M., McInnes, R.R., 2003. Progress toward understanding the genetic and biochemical mechanisms of inherited photoreceptor degenerations. Annu. Rev. Neurosci. 26, 657–700.

Postlethwait, J.H., Woods, I.G., Ngo-Hazelett, P., Yan, Y.L., Kelly, P.D., Chu, F., Huang, H., Hill-Force, A., Talbot, W.S., 2000. Zebrafish comparative genomics and the origins of vertebrate chromosomes. Genome Res. 10, 1890–1902.

Rachel, R.A., Mason, C.A., Beermann, F., 2002. Influence of tyrosinase levels on pigment accumulation in the retinal pigment epithelium and on the uncrossed retinal projection. Pigm. Cell Res. 15, 273–281.

Rando, R.R., 2001. The biochemistry of the visual cycle. Chem. Rev. 101, 1881–1896.

Raposo, G., Tenza, D., Berson, J.F., Harper, D., Theos, A., Marks, M.S., 2003. IL-26 The biogenesis of melanosomes in highly pigmented cells. Pigm. Cell Res. 16, 584.

Ratnaswamy, G., Koepf, E., Bekele, H., Yin, H., Kelly, J.W., 1999. The amyloidogenicity of gelsolin is controlled by proteolysis and pH. Chem. Biol. 6, 293–304.

Rodieck, R.W., 1998. The First Steps in Seeing. Sinauer Associates.

Schmitt, E.A., Dowling, J.E., 1999. Early retinal development in the zebrafish, *Danio rerio*: light and electron microscopic analyses. J. Comp. Neurol. 404, 515–536.

Schraermeyer, U., Heimann, K., 1999. Current understanding on the role of retinal pigment epithelium and its pigmentation. Pigm. Cell Res. 12, 219–236.

Schulte-Merker, S., 2002. Looking at embryos. In: Nusslein-Volhard, C., Dahm, R. (Eds.), Zebrafish, Practical Approach Series. Oxford Univ. Press, pp. 39–58.

Shimoda, N., Knapik, E.W., Ziniti, J., Sim, C., Yamada, E., Kaplan, S., Jackson, D., de Sauvage, F., Jacob, H., Fishman, M.C., 1999. Zebrafish genetic map with 2000 microsatellite markers. Genomics 58, 219–232.

Steinberg, R.H., 1985. Interactions between the retinal pigment epithelium and the neural retina. Doc. Ophthalmol. 60, 327–346.

von Lintig, J., Vogt, K., 2000. Filling the gap in vitamin A research. Molecular identification of an enzyme cleaving beta-carotene to retinal. J. Biol. Chem. 275, 11915–11920.

von Lintig, J., Vogt, K., 2004. Vitamin A formation in animals: molecular identification and functional characterization of carotene cleaving enzymes. J. Nutr. 134, 251S–265S.